MAX-PLANCK-INSTITUT FÜR PLASMAPHYSIK

GARCHING BEI MÜNCHEN

Whistler dominated quasi-collisionless magnetic reconnection

Dieter Biskamp and James F. Drake

IPP 6/328 May 1995

Die nachstehende Arbeit wurde im Rahmen des Vertrages zwischen dem Max-Planck-Institut für Plasmaphysik und der Europäischen Atomgemeinschaft über die Zusammenarbeit auf dem Gebiete der Plasmaphysik durchgeführt.

Whistler dominated quasi-collisionless magnetic reconnection

D. Biskamp[1] and J.F. Drake[2]
[1]Max-Planck-Institut für Plasmaphysik,
D-85748 Garching, Germany
[2]Institute for Plasma Research, University of Maryland,
College Park, Maryland 20742, USA

Abstract

A theory of fast quasi-collisionless reconnection is presented. For spatial scales smaller than the ion inertia length the electrons decouple from the ions and the dynamics is described by electron magnetohydrodynamics (EMHD). A qualitative analysis of the reconnection region is obtained, which is corroborated by numerical simulations. The main results are that in contrast to resistive reconnection no macroscopic current sheet is generated, and the reconnection rate is independent of the smallness parameters of the system, i.e. the electron inertia length and the dissipation coefficients. At larger scales the coupling to the ions is important, which, however, does not change the small-scale dynamics. The reconnection rate is only limited by ion inertia being independent of the electron inertia scale and the dissipation coefficients. Reconnection is much faster than in the absence of the whistler mode.

1 Introduction

It has been realized since some time that fast magnetic reconnection processes may occur in nearly collisionless plasmas. For instance the observed time scales in the sawtooth collapse in tokamak plasmas [1] are much faster than could be accounted for by the weak collisional effects such as resistivity or electron viscosity. Even more stunning are the rapid processes observed in the extraterrestrical environment, magnetospheric substorm, which seem to be caused by reconnection in the magnetotail plasma, and solar flares with reconnection occuring in the solar corona, both plasmas being virtually collisionless.

Recently several theoretical and numerical investigations indicate that the nondissipative terms in Ohm's law usually discarted in reconnection theory [5], in particular electron inertia [2] and electron pressure [3], may give rise to very high reconnection rates. Numerical simulations have also shown, that the Hall term, which introduces the whistler mode, may lead to rapid reconnection [4]. These processes are, however, not yet well understood. What is the mechanism for the high reconnection rate, and what is the structure of the reconnection region in the limit of almost vanishing dissipation? In this paper we consider the generalized Ohm's law for low-β plasmas including both electron inertia and the Hall term but neglecting the electron pressure effect. (The latter, which is important in high-β plasmas, has recently been studied [6].) In section 2 we introduce the equations of electron magnetohydrodynamics (EMHD), which are valid at sufficiently small spatial and time scales, where the ions can be considered immobile. In section 3 we develop a qualitative theory of reconnection in the framework of EMHD, which accounts for the possibility of fast reconnection independent of the smallness parameters, i.e. the electron inertia length c/ω_{pe} and the dissipation coefficients. Section 4 gives the results of numerical simulations of the coalescence of two flux bundles, which essentially confirm the theory outlined in section 3. For sufficiently weak dissipation the electron flow along the layer excites small-scale whistler turbulence, which leads to finite energy dissipation in the collisionless limit. The properties of the turbulence are discussed in section 5. In section 6 the coupling of the EMHD equations to the ion fluid is introduced, for which we derive a simple set of equations. Numerical simulations at finite c/ω_{pi} show that the EMHD reconnection dynamics for scales $< c/\omega_{pi}$ is essentially preserved. The reconnection rate depends only on the ion inertia, being independent of c/ω_{pe} and the dissipation coefficients. The importance of the Hall term is demonstrated by repeating the simulations with this term switched off. Section 7 sumarizes the results.

2 The EMHD equations

On spatial scales smaller than the ion inertia length c/ω_{pi} the ions can no longer follow the dynamics. They form a static charge-neutralizing background, which can be assumed homogeneous. Under these conditions the dynamics is only due to electron motions in their selfconsistent magnetic fields, which in the simplest approximation is described by the equations of EMHD, the main assumptions being isotropic pressure, homogeneous density and the omission of the displacement current. EMHD has recently been discussed in several articles [7], [8], [9]. The equations consist of the electron equation of motion for $\mathbf{v}_e = -\mathbf{j}/en$,

$$\frac{4\pi}{\omega_{pe}^2}\left(\partial_t \mathbf{j} + \mathbf{v}_e \cdot \nabla \mathbf{j}\right) = \mathbf{E} - \frac{1}{nec}\mathbf{j} \times \mathbf{B} + \frac{1}{ne}\nabla p_e + \mathbf{D}_e \ , \tag{1}$$

and Faraday's law

$$\partial_t \mathbf{B} = -c\nabla \times \mathbf{E} \ , \tag{2}$$

where $\mathbf{D}_e$ represents resistive and viscous dissipation, and $\mathbf{j}$ and $\mathbf{B}$ are coupled by Ampère's law

$$\nabla \times \mathbf{B} = \frac{4\pi}{c}\mathbf{j} \ . \tag{3}$$

Eliminating $\mathbf{E}$, assuming constant density, gives

$$\partial_t \left(\mathbf{B} - d_e^2 \nabla^2 \mathbf{B}\right) - \nabla \times \left[\mathbf{v}_e \times \left(\mathbf{B} - d_e^2 \nabla^2 \mathbf{B}\right)\right] = c\nabla \times \mathbf{D}_e \tag{4}$$

with $d_e = c/\omega_{pe}$. Note that the pressure p_e does not appear in the final equation (4). Linearization about a constant magnetic field $\mathbf{B}_0$ yields the dispersion relation of whistler modes

$$\omega^2 = \Omega_e^2 d_e^4 k_{\|}^2 k^2 / \left(1 + d_e^2 k^2\right)^2 \ , \tag{5}$$

where $\Omega_e = eB_0/m_e c$ is the electron cyclotron frequency. For $kd_e \lesssim 1$ eq. (5) describes modes with high group velocity $v_g = \partial\omega/\partial k \sim k$, the whistler mode proper, while for $kd_e > 1$ the whistler frequency approaches $\omega \simeq \Omega_e$, such that the group velocity becomes very small. Hence a behavior basically different from incompressible MHD is possible, where linear modes are nondispersive Alfvén waves $\omega^2 = k_{||}^2 v_A^2$.

Whistler modes are destabilized by a strong current density gradient [10]. In the presence of a large field B_0 (low-β plasma), where electric currents are essentially parallel to $\mathbf{B}_0$, the most unstable modes $\mathbf{k}$ are in the plane perpendicular to $\mathbf{B}_0$. This behavior suggests to study whistler-related processes in this plane. Choosing $\mathbf{B}_0 = B_0 \hat{\mathbf{z}}$, the 2D version of eq. (4) can be written in terms of the flux function ψ for the poloidal field $\mathbf{B}_\perp = \hat{\mathbf{z}} \times \nabla\psi$, and the axial field fluctuation $B_z - B_0 = \varphi_e$, where the notation indicates that φ_e acts as a streamfunction of the poloidal electron velocity, $\mathbf{v}_e = \hat{\mathbf{z}} \times \nabla\varphi_e$,

$$\begin{aligned} \partial_t \left(\psi - d_e^2 j\right) + \mathbf{v}_e \cdot \nabla \left(\psi - d_e^2 j\right) &= \eta_\nu \left(-\nabla^2\right)^\nu \psi \, , &(6)\\ \partial_t \left(\varphi_e - d_e^2 \omega_e\right) - d_e^2 \mathbf{v}_e \cdot \nabla\omega_e + \mathbf{B}_\perp \cdot \nabla j &= \eta_\nu \left(-\nabla^2\right)^\nu \varphi_e \, , &(7)\\ j = \nabla^2\psi \, , \quad \omega_e = \nabla^2\varphi_e \, . \end{aligned}$$

Equations (6), (7) are written in nondimensional form, where we have used the normalizations $\hat{x} = x/L$, $\hat{t} = t/(L^2/\alpha B_{\perp 0})$, $\hat{\varphi}_e = \varphi_e/B_{\perp 0}$, $\hat{d}_e = c/\omega_{pe}L$, $\hat{\eta}_\nu = \eta_\nu/\alpha B_{\perp 0} L^{2(\nu-1)}$, finally leaving off the hat in the notation. $\alpha = c/4\pi ne$ is the Hall constant, $\alpha B_{\perp 0} = d_e^2 \Omega_e$, $B_{\perp 0}$ is a typical poloidal field (the axial field B_0 does not appear in the 2D equations) and L a typical poloidal scale. Note that the time unit, the whistler time $t_W = L^2/\alpha B_{\perp 0}$, differs from the Alfvén time $t_A = L/v_A$, $v_A = B_{\perp 0}/\sqrt{4\pi n m_i}$, conventionally used in MHD theory, $t_W = t_A/d_i$.

In eqs. (6), (7) we have introduced generalized dissipation coefficients η_ν, where η_1 corresponds to the normal resistivity, η_2 to (perpendicular) electron viscosity. The equations are formally similar to 2D incompressible MHD. Equation (6) expresses the conservation of the canonical momentum in z direction replacing that of the magnetic flux in the MHD case. φ_e and ω_e are streamfunction and vorticity of the electron flow $\mathbf{v}_e$, analogous to φ_i and $\omega_i = \nabla^2\varphi_i$ of the ion (=mass) flow in MHD. It should also be mentioned that in eq. (6), which results from integration of eq. (4), a gradient corresponding to $\nabla_{||} p_e$ is neglected.

Let us briefly indicate the important conservation laws satisfied by eqs. (6), (7). In the dissipationless limit the following quantities are conserved : the total energy,

$$W = \tfrac{1}{2} \int \left[\varphi_e^2 + (\nabla \psi)^2 + d_e^2 \left((\nabla \varphi_e)^2 + j^2 \right) \right] dV \ , \tag{8}$$

the "cross helicity"

$$K = \tfrac{1}{2} \int \left(\psi - d_e^2 j \right) \left(\varphi_e - d_e^2 \omega_e \right) dV \ , \tag{9}$$

the generalized flux

$$\Phi = \int f \left(\psi - d_e^2 j \right) dV \ , \tag{10}$$

where $f(x)$ is an arbitrary function, and a quantity

$$G = \tfrac{1}{2} \int \left(\psi^2 - d_e^2 (\nabla \psi)^2 - d_e^2 \left(\varphi_e^2 + d_e^2 (\nabla \varphi_e)^2 \right) \right) dV \ , \tag{11}$$

the meaning of which is not obvious. We can, however, not exclude that further invariant quantities exist.

3 Whistler mediated reconnection

In this section we consider the problem of stationary reconnection in the framework of the EMHD equations (6), (7). The case of vanishing inertia $d_e \to 0$ has recently been treated numerically by Mandt et al. [4], who consider the coalescence of two flux bundles. It is found that the average reconnection rate is fast independent of the value of the resistivity. Here we generalize the result to finite d_e. We present a qualitative treatment of the stationary reconnection configuration around the X-point. The results are essentially confirmed by numerical simulations in section 4. We start by noting that for $d_e = 0$, i.e. for $|x| \gg d_e$, the stationary equations (6), (7)

$$\begin{aligned} E + \mathbf{v}_e \cdot \nabla \psi &= 0 \ , && (12) \\ \mathbf{B}_\perp \cdot \nabla j &= 0 && (13) \end{aligned}$$

have the similarity solution

$$\begin{aligned} \psi &= \tfrac{1}{2} \left(x^2 - y^2 \right) \ , && (14) \\ \varphi_e &= \frac{E}{2} \ln \left| \frac{x+y}{x-y} \right| \ , && (15) \end{aligned}$$

where $E = \partial_t \psi$ is a free parameter. The upstream flow converges toward the X-point and the downstream flow diverges away from it. Finite resistivity is only needed to smooth the flow singularity on the separatrix $x = \pm y$. (By contrast in MHD the solution (14), (15) is found to be only valid for sufficiently small reconnection rate [11].)

In the vicinity of the neutral point electron inertia in eq. (7) is no longer negligible and the electron flow deviates from the similarity solution (15). The magnetic flux, on the other hand, is essentially unaffected by the inertia term, the X-point configuration (14) remaining valid also in the inertia-dominated region close to the neutral point. This invariance of ψ, which differs from the behavior in MHD, originates from Ampère's law connecting j and ψ, since the electron velocity determines the current density. From the canonical momentum $F(x,y) = \psi - d_e^2 \nabla^2 \psi$ we find by integration using the appropriate Green's function, that

$$\psi = \int G\left(\frac{x-x'}{d_e}, \frac{y-y'}{d_e}\right) F(x',y')\, d^2x' \,, \tag{16}$$

which implies that ψ varies only on scales $> d_e$, i.e. is not affected by the current distribution inside the inertia-dominated region. Hence ψ can be assumed given by eq. (14). This allows a rather complete qualitative discussion of the dynamic behavior in this region.

Let us first estimate the scale l, where the electron inertia term becomes important in eq. (7). We assume that dissipative effects are sufficiently small, such that the dissipative terms are negligible on the scale l. Hence eq. (6) reads

$$\mathbf{v}_e \cdot \nabla \left(\psi - d_e^2 \nabla^2 \psi\right) = -E$$

For $x \sim l$ both terms on the left side are of the same order of magnitude, the first one dominating at larger scales, the second at smaller scales,

$$v_{ex} B_y \sim v_{ex} d_e^2\, j/l, \quad v_{ex} B_y \sim E \,. \tag{17}$$

Integrating eq. (7) and neglecting the electron pressure gives

$$d_e^2 v_{ex} \partial_x v_{ex} \sim d_e^2\, v_{ex}/l \sim j B_y \,. \tag{18}$$

With $B_y(l) = l$ from eq. (14) eqs. (17), (18) yield the scale

$$l \sim \left(d_e^2 E\right)^{1/3} \,. \tag{19}$$

(A similar result has been obtained in ref. [12].) Inside the region l the current density increases toward the X-point until dissipative effects become important forming a narrow layer $\delta < l$. It is important to note the electron inertia does not prevent the formation of singular structures. The vorticity is concentrated in the layer δ. Hence for $\delta < x < l$ the flow is essentially irrotational. Using the notations $v_{ex}(l) = u_0$, $v_{ex}(\delta) = u_1$, the simplest irrotational solution in this region is (see Fig. 1)

$$\varphi_e = (u_0 - u_1)\frac{x}{l}y + u_1 y \ , \tag{20}$$

where u_0 is obtained from eq. (15)

$$u_0 = \frac{E}{l} \ , \tag{21}$$

and $u_0\,\delta/l < u_1 < u_0$. Integrating eq. (6) in this region,

$$E = -v_{ex}\partial_x\left(\psi - d_e^2 j\right) \simeq v_{ex} d_e^2 \partial_x j \ , \tag{22}$$

along the x-axis using expression (20) gives the current density j_m in the layer $x \lesssim \delta$

$$\begin{aligned} j_m &= \frac{E}{u_0 - u_1}\frac{l}{d_e^2}\ln\frac{u_0}{(u_0-u_1)\frac{\delta}{l} + u_1} \\ &\simeq \frac{l^2}{d_e^2}\ln\frac{u_0}{u_1} \\ &= \left(\frac{E}{d_e}\right)^{2/3}\ln\frac{u_0}{u_1} \end{aligned} \tag{23}$$

using relations (19) and (21).

To calculate the variation of j along the the layer we use the conservation of the canonical momentum $\partial_y(\psi - d_e^2 j) = 0$ and eq. (14) :

$$j(y) = j_m - \frac{y^2}{2d_e^2} \ . \tag{24}$$

The length Δ of the current layer is defined by $j(\Delta) = 0$, which coincides with the point, where the outflow velocity reaches its maximum value v_0 (in general the layer edge has a rather complicated structure with positive and negative current density parts, see also section 5). Equations (23) and (24) give

$$\Delta \sim \left(d_e^2 E\right)^{1/3} \sim l \ , \tag{25}$$

neglecting the logarithmic factor. Hence we find the important result that the length of the layer decreases with d_e, which implies that there is no macroscopic current sheet in contrast to the behavior in resistive MHD [11].

We now integrate eq. (7) over the area of the layer δ, indicated in Fig. 2. By applying Gauss's theorem we obtain neglecting the dissipation term

$$d_e^2 \oint v_{en} \omega_e dl = \oint B_n j dl \ . \tag{26}$$

Since $\omega_e = 0$ on the paths 1 and 2 (exactly) and 4 (approximately), only 3 contributes to the integral on the left side, while the major contribution to the right side comes from path 2.

$$d_e^2 \int_3 v_y \partial_x v_y dx = \int_2 j \partial_y \psi dy = d_e^2 \int_2 j \partial_y j dy \tag{27}$$

making use of $\psi - d_e^2 j = const$ along the layer. Since the outflow velocity v_0 in the layer is much larger than outside the layer, eq. (27) gives the relation

$$v_0 \simeq j_m \ . \tag{28}$$

This implies that the electron velocity $v_{ey} = v_0$ at the layer edge equals the velocity $v_{ez} = j$ in the center. This behavior, which is a consequence of the conservation of the canonical momentum, can be interpreted as a gyromotion in the field $B_x \sim d_e$ perpendicular to the sheet. Equation (28) should be contrasted with the MHD behavior $v_0 \simeq v_A$ in a Sweet-Parker sheet, where v_A is the Alfvén speed corresponding to ΔB, the jump across the sheet.

Finally, the sheet width δ can be estimated by considering eq. (6) at the stagnation point

$$E = \eta_\nu \left(-\nabla^2\right)^\nu \psi \sim \eta_\nu \frac{j}{\delta^{2(\nu-1)}} \ ,$$

hence

$$\delta \sim \left(\eta_\nu \frac{j}{E}\right)^{\frac{1}{2(\nu-1)}} \sim \eta_\nu^{\frac{1}{2(\nu-1)}} \ , \tag{29}$$

since j and E vary only weakly with η_ν.

To summarize the results of this section, we have shown or at least made plausible that the external solution (14), (15) can be matched to the internal solution in the inertia-dominated region for any value of E. Hence the reconnection rate in EMHD should be independent of the smallness parameters d_e and η_ν, depending only on the global magnetic configuration. Numerical simulations, considered in the following section, essentially confirm these predictions.

4 Coalescence of flux bundles in EMHD

The coalescence of two flux bundles (flux tubes, magnetic islands) is probably the best known paradigm of a fast selfconsistent reconnection process. We consider two flux bundles located on the diagonal in a square box of linear size 2π with periodic boundary conditions :

$$\begin{aligned}\psi = a_1 \exp\left\{-\left[\frac{(x-x_1)^2+(y-y_1)^2}{2x_0^2}\right]^2\right\} \\ +a_2 \exp\left\{-\left[\frac{(x-x_2)^2+(y-y_2)^2}{2x_0^2}\right]^2\right\} - \psi_0\ ,\end{aligned} \tag{30}$$

where the constant ψ_0 is chosen to make $\langle\psi\rangle = 0$, $x_1 = y_1 = \pi/2 + 0.2$, $x_2 = y_2 = 3\pi/2 - 0.2$ and $x_0 = 1.0$ or 1.1. To avoid perfect symmetry, which tends to suppress certain turbulent motions, we consider also the case, where the weight factors a_1, a_2 are chosen slightly different $a_1 = 0.9$, $a_2 = 1.1$, and in addition a low level random velocity field $\tilde{\varphi}_e(x,y)$ is imposed initially.

With these initial conditions eqs. (6), (7) are solved numerically with a pseudo-spectral method and dealiasing according to the 2/3 rule. The number of modes (more appropriately collocation points) N^2 is chosen suitably to provide adequate numerical resolution, N varying between 256 and 2048. Numerical resolution is controlled by inspection of the energy spectrum, which should exhibit an exponential drop in the high-k dissipation range of at least a factor of 10. Resistivity η_1 is in general not sufficient to prevent the formation of singularities, since for $\nu = 1$ the dissipation terms reduce to friction terms in j and ω_e. Hence we choose $\nu > 1$, in most cases $\nu = 3$ in order to concentrate the dissipative effects to the highest wave numbers.

A number of simulation runs have been performed with different values of the parameters d_e and η_3. Figure 3 gives the time evolution of the flux $\psi(t)$ at the X-point and the reconnection rate $E = \partial_t \psi$ for three different cases. The reconnection process is essentially identical in the three cases, E increasing in time and subsequently decaying as coalescence reaches completion. Figure 4 shows ψ and φ_e at two times $t = 0.6$ and $t = 1.1$ during the coalescence process for the case with $d_e = 0.03$, $\eta_3 = 10^{-8}$. The conspicuous feature is that the flux surfaces appear to be pulled into the central reconnection region instead of pushed against it as in the MHD case. This property is due to the flow pattern with stream lines converging (i.e. velocity increasing) toward the X-point, which agrees with the similarity solution (15). (In the MHD case the flow is rather uniform across the flux bundle, even diverging in front of the macroscopic current sheet.)

Table 1 gives the maximum value E_{max} for seven different cases. The numbers confirm, that the reconnection rate is essentially independent of both d_e and the value of the dissipation coefficient (apart from a weak *increase* with decreasing d_e).

The properties of the reconnection region are illustrated in Table 2, where the measured values of the characteristic quantities are given from three simulation runs taken at the same instant $t = 0.64$. It can be seen that the numerical results agree approximately with the theoretical predictions, l seems to depend on d_e somewhat more strongly, $l \sim d_e^{0.9}$, than predicted in eq. (19), while Δ follows the predicted law $\Delta \sim d_e^{2/3}$. Relation (28) is well satisfied. The increase of j_m with decreasing dissipation coefficient can be related with the decrease of δ and hence u_1 in the logarithmic factor in eq. (23). Also the E-dependence of j_m is approximately recovered considering the time variation of j_m during the increase of $E(t)$ as seen in Fig. 3. The differences between the analytical and the simulation results may be attributed to the fact that the numerical configuration around the X-point is still affected by the global current distribution and that the analytical solution is oversimplified neglecting for instance the current and vorticity contributions from the separatrix.

Hence we find that the numerical simulations support the main results of the theory of section 3. The electron flow is accelerated toward the X-point; the reconnection rate is independent of the details of the reconnection process, in particular does not depend on d_e and the dissipation coefficients; the layer length Δ shrinks with d_e, such that there is no macroscopic current sheet.

5 Whistler turbulence generated in collisionless reconnection

It is known from MHD reconnection theory [11], that for sufficiently small resistivity the strong collimated flow along the current sheet generates a complex behavior, when entering the low-field downstream region. In EMHD, where the flow is even much stronger compared with the adjacent magnetic field, strong whistler turbulence is generated, which propagates into the downstream region. This behavior is illustrated in Fig. 5, which shows results from a more general reconnection process developing from the initial state A_1 from Ref. [14] (with $\varphi \to \varphi_e$), with $d_e = 0.03$, $\eta_3 = 10^{-11}$. Reconnection occurs in four points as seen in Fig. 5b. The remaining frames Fig. 5c-e give blowups of the region around the lower right reconnection point, showing ψ, j and ω_e. One can clearly recognize that the turbulence is generated by $\mathbf{v}_e$, the current along the sheet, and not by j, the out of plane current.

The mechanism of turbulence excitation can be identified with the Kelvin-Helmholtz instability of the electron flow. Since turbulence wavelengths are short $k \sim \delta^{-1} \gg d_e^{-1}$, and $\omega_e \gg j$, eq. (7) reduces to the 2D Euler equation. Kelvin-Helmholtz instability arises, roughly speaking, if $kl_s < 1$, where l_s is the scale of the velocity shear and k the wavenumber, and $\gamma \sim v/l_s$ is a typical growth rate. In our case $v \sim v_0$ and $l_s \sim \delta$. Instability becomes manifest if the sheet aspect ratio Δ/δ is sufficiently large. (In a more rigorous treatment dissipation must be included, which is not negligible on the scale δ and which raises the instability threshold.) The instability first appears at the sheet edge, but as δ becomes smaller by lowering the dissipation coefficients the entire sheet is affected.

The resulting turbulence exhibits some interesting properties. We consider again the initial state A_1 from ref. [14], but choose $d_e = 1$, such that long sheets develop, $\Delta \gtrsim 1$, with a particularly large aspect ratio Δ/δ. These sheets are violently unstable (Fig. 6a,b) leading to quasi-stationary turbulence (Fig. 6c) which occupies most of the area. The energy spectrum (Fig. 7) has an extended inertial range, which follows the Kolmogorov law $k^{-5/3}$ very closely. The energy dissipation rate $\varepsilon = -dW/dt$ is nearly constant for a time much longer than the formation period and is independent of the values of the dissipation coefficients. In spite of the fact that in eq. (7) the term $\mathbf{B}\cdot\nabla j$ is in general much smaller than the convective term $\mathbf{v}_e\cdot\nabla\omega_e$, the former plays a crucial role as a source of vorticity, which in the absence of this term could only decay. To demonstrate this effect, we switch off ψ at $t=4$ and let ω_e develop freely up to time $t=6$. The vorticity field soon assumes a state consisting of isolated vortices (Fig. 8), which is characteristic of decaying 2D Navier-Stokes turbulence (the energy spectrum is about k^{-4}) and is much different from the EMHD turbulence state in Fig. 6c.

6 Coupling to finite mass ions

In EMHD the ions are assumed to be infinitely massive. This approximation is only valid for magnetic structures of scales smaller than the ion inertial length c/ω_{pi}. In most practical applications, however, the global scales of the magnetic eddies involved in reconnection processes are much larger, so that the coupling to the ions cannot be neglected. On scales $> c/\omega_{pi}$ ions and electrons essentially move together, which justifies neglecting the Hall term $\frac{1}{cen}\mathbf{j}\times\mathbf{B}$ compared with the ion contribution $\frac{1}{c}\mathbf{v}_i\times\mathbf{B}$ in MHD. It is therefore important to investigate to what extend the coupling to finite mass ions affects the reconnection dynamics of EMHD just discussed.

We introduce the ion streamfunction φ_i, $\mathbf{v}_i=\hat{\mathbf{z}}\times\nabla\varphi_i$, $\omega_i=\nabla^2\varphi_i$. Adding the ion and the electron fluid equation gives

$$\begin{aligned} d_i^2\left(\partial_t\omega_i+\mathbf{v}_i\cdot\nabla\omega_i\right)+d_e^2\left(\partial_t\omega_e+\mathbf{v}_e\cdot\nabla\omega_e\right)-\mathbf{B}_\perp\cdot\nabla j \\ =(-1)^\nu\left[\mu_\nu\nabla^{2(\nu-1)}\omega_i+\eta_\nu\nabla^{2(\nu-1)}\omega_e\right] , \end{aligned} \tag{31}$$

using the normalization introduced in section 2, $d_i=c/\omega_{pi}L$. Neglecting the out-of-plane ion motion (essentially the motion along the assumed strong field B_0), the out-of-plane current density j remains unchanged and so does the equation for ψ, eq. (6). The current density in the plane is, however, modified, $\mathbf{j}_\perp=-\hat{\mathbf{z}}\times\nabla b=\hat{\mathbf{z}}\times\nabla\varphi_i-\hat{\mathbf{z}}\times\nabla\varphi_e$. Hence we find $b=\varphi_e-\varphi_i$ which must be substituted for φ_e in eq. (7). Noting that the electron inertia term contains only the electron flow φ_e, eq. (7) becomes

$$\begin{aligned} \partial_t\left(\varphi_e-\varphi_i-d_e^2\omega_e\right)+\mathbf{v}_e\cdot\nabla\left(\varphi_e-\varphi_i-d_e^2\omega_e\right)+\mathbf{B}_\perp\cdot\nabla j \\ =(-1)^\nu\eta_\nu\nabla^{2(\nu-1)}\omega_e . \end{aligned} \tag{32}$$

The energy expression now also contains the ion contribution

$$W = \frac{1}{2} \int \left[b^2 + (\nabla\psi)^2 + d_e^2 \left((\nabla\varphi_e)^2 + (\nabla^2\psi)^2 \right) + d_i^2 (\nabla\varphi_i)^2 \right] dV \; , \qquad (33)$$

where $b = \varphi_e - \varphi_i$ is understood.

Since it is numerically difficult to combine the most interesting case $d_i \ll 1$ with a realistic ratio $d_i/d_e = \sqrt{m_i/m_e} \sim 50$, we choose values $d_i/d_e \sim 10$, varying both d_i, $0.4 \geq d_i \geq 0.05$, and d_i/d_e, $13.3 \geq d_i/d_e \geq 6.6$, to obtain the relevant scaling laws. Figure 9 shows a typical state from a simulation run with $d_i = 0.05$, $d_e = 0.0075$, $\eta_3 = 4 \times 10^{-10}$. It can be seen by comparing φ_e and φ_i contours, Figs 9b,c, that at large distances from the X-point and the separatrix ion and electron flow patterns are very similar. They differ, however, in the vicinity of the X-point (and along the separatrix), where typical ion scale lengths are much larger than those of the electrons, being connected with d_i and d_e, respectively. For $d_i > |x| > d_e$ the electron flow behaves as in EMHD. We find that the maximum velocities v_{im}, v_{em} reached in the downstream cone roughly scale as $v_{em}/v_{im} \sim d_i/d_e$ and so do the distances Δ_i, Δ_e from the X-point, where these velocities are reached, $\Delta_i/\Delta_e \sim d_i/d_e$. It is also noteworthy that at the separatrix the ion velocity changes abruptly in a shock-like way from the lower inflow to the higher outflow values. This behavior is reminiscent of the Petschek configuration, which can be set up in this fast reconnection process in contrast to slow resistive reconnection.

As seen from Table 3 the reconnection rate depends only on d_i, i.e. ion inertia, while it is independent of d_e and the values of the dissipation coefficients. The fact that in Table 3 the reconnection rate, in particular E_{max}, increases with decreasing d_i, is due to the normalization to the whistler time t_W, connected to the Alfvén time by $t_A = t_W d_i$. Hence the scaling $E_{max} \sim d_i^{-1}$ obtained from Table 3 for the range $1 > d_i \gtrsim 0.1$ implies that reconnection proceeds on the Alfvén time scale depending only on the global configuration.

It should be noted that the state shown in Fig. 9 illustrates the behavior of the coalescence process for $t \lesssim t_m$ with $E(t_m) = E_{max}$, where the time variation of $E(t)$ is similar to that in the pure EMHD cases given in Fig. 3. In this phase, where roughly half of the available magnetic flux is reconnected, reconnection is quasi-Alfvénic. At later times $t > t_m$ E decreases, while the flow velocities, i.e. the kinetic energy, is still growing, since the magnetic energy continues to decrease until coalescence is complete. In this phase the inflow velocity is too high to be matched by the decreasing rate of flux removal such that flux is piled up in front of the layer, the length of which increases to macroscopic size. This stretched-out sheet becomes unstable to plasmoid generation similar to the behavior in the resistive case [11]. Reconnection in this second phase is not slow, since plasmoid generation is accompanied by the reconnection at newly arising X-points, which is as efficient as at the original central X-point in the first phase. The quasi-collisionless behavior in the limit $d_i \to 0$ is difficult to assess. The system will probably be rather turbulent in the reconnection region involving both electron whistler turbulence as discussed in section 5 and MHD turbulence. In any case will reconnection be much faster than predicted by theories ignoring the Hall term.

To demonstrate the role of the whistler dynamics we switch off the Hall term by setting $\varphi_e = \varphi_i = \varphi$, but keep finite electron inertia in eq. (6). This model has previously been used in studies of collisionless reconnection, e.g. [2], [13]. Figure 10 illustrates the resulting behavior for a run with $d_i = 0.2$, $d_e = 0.015$. (Note that neglecting the Hall term eliminates the ion inertia scale c/ω_{pi} as an independent spatial scale, as can be seen by writing the equations with the conventional Alfvén time normalization.) Compared with Fig. 9 the flow pattern is changed significantly, the ions are now forced into a layer of width d_e. The reconnection rate is found to be much slower than in the corresponding case including the Hall term. Varying d_e we find that the reconnection dynamics depends strongly on d_e, roughly $E_{max} \sim d_e$.

7 Conclusions

We have shown that the Hall term in Ohm's law has an important effect on the dynamics of magnetic reconnection processes in almost collisionless plasmas, leading to reconnection rates which are essentially independent of the smallness parameters, the electron inertia length and the weak dissipation effects, depending only on the ion inertia. Neglecting the Hall term, but keeping electron inertia, which has often been considered to be the most important collisionless effect in Ohm's law, leads to a much slower reconnection rate $E \sim d_e$. It is interesting to note that the Hall term, which contributes to $E_\perp$, appears to be more important than $E_{||}$, which is usually considered as the essential mechanism for reconnection. Though reconnection requires finite $E_{||}$, the reconnection *dynamics* depends also on the dispersive properties of the system which are strongly affected by the Hall term. In MHD theory the only relevant linear mode is the nondispersive Alfvén wave $\omega^2 = k_{||}^2 v_A^2$, where group and phase velocities are independent of k depending only on the direction of $\mathbf{k}$ with respect to the magnetic field. Strong stationary field gradients can be generated perpendicular to the field, since the group velocity vanishes. Since along the field, i.e. along the current sheet the fluid velocity increases, there can be no small-scale stationary spatial structure, hence the sheet extends to macroscopic length. The Hall term introduces a highly dispersive mode, the whistler, eq. (5). Neglecting electron inertia $d_e \to 0$ an inhomogeneous stationary configuration is given by eqs (14), (15). Since the fluid velocity decreases away from the X-point $v \sim \frac{1}{|\mathbf{x}|}$, the group velocity $v_g \sim k$ can match the structure of this configuration $k \sim \frac{1}{|\mathbf{x}|}$. This is no longer true for modes $kd_e > 1$ where $v_g \sim k^{-3}$. For such small-scale structures to be stationary v has to increase, i.e. there must be a sheet of length d_e.

We should mention that a similar situation arises when instead of the Hall term the electron pressure term in Ohm's law is taken into account, which leads to a different dispersive mode, the kinetic Alfvén wave. In this case we also expect a macroscopic X-point behavior giving rise to fast reconnection, which is essentially confirmed numerically [3], [6].

References

[1] see e.g. A.M. Edwards et al., Phys. Rev. Lett. **57**, 210 (1986)

[2] M. Ottaviani and F. Porcelli, Phys. Rev. Lett. **71**, 3802 (1993)

[3] A.Y. Aydemir, Phys. Fluids **B4**, 3469 (1992)

[4] M.E. Mandt, R.E. Denton, and J.F. Drake, Geophys. Res. Lett. **21**, 73 (1994)

[5] see e.g. D. Biskamp, Phys. Rep. **237**, 181 (1994)

[6] R.G. Kleva, J.F. Drake, and F.L. Waelbroeck, Phys. Plasmas **2**, 23 (1995)

[7] A.S. Kingsep, K.V. Chukbar, and V.V. Yan'kov, in *Reviews of Plasma Physics* (Consultants Bureau, New York, 1990), Vol. 16

[8] S.V. Bulanov, F. Pegoraro, and A.S. Sakharov, Phys. Fluids **B4**, 2499 (1992)

[9] J.F. Drake, R.G. Kleva, and M.E. Mandt, Phys. Rev. Lett. **73**, 1251 (1994)

[10] A.B. Mikhailowskii, *Theory of Plasma Instabilities* (Consultants Bureau, New York, 1974), Vol. 2; M.J. Keskineu and J.D. Huba, J. Geophys. Res. **88**, 3109 (1983)

[11] D. Biskamp, Phys. Fluids **29**, 1520 (1986)

[12] G.R. Burkhart, J.F. Drake, and J. Chen, J. Geophys. Res. **95**, 18833 (1990)

[13] J.F. Drake and R.G. Kleva, Phys. Rev. Lett. **66**, 1458 (1991)

[14] D. Biskamp and H. Welter, Phys. Fluids, **B1**, 1964 (1989)

d_e	η_3	E_{max}
0.1	10^{-6}	1.28
0.1	10^{-8}	1.30
0.06	10^{-8}	1.27
0.06	5×10^{-10}	1.36
0.03	10^{-8}	1.42
0.03	5×10^{-10}	1.42
0.01	10^{-8}	1.53

Table 1 Maximum reconnection rate E_{max} for seven different EMHD runs.

d_e	η_3	l	Δ	v_0	j_m
0.06	5×10^{-10}	0.031	0.12	5.4	6.3
0.03	5×10^{-10}	0.016	0.08	5.5	6.7
0.03	5×10^{-11}	0.018	0.077	7.6	8.5
0.015	5×10^{-11}	0.01	0.05	8.1	11.5

Table 2 Characteristic quantities of the reconnection region for three different EMHD runs.

d_i	d_e	η_3	E_{max}	t_0
∞	0.03	10^{-8}	1.4	1.5
0.4	0.03	4×10^{-10}	1.7	1.3
0.2	0.03	10^{-8}	2.5	1.0
0.2	0.015	10^{-8}	2.4	1.0
0.2	0.03	4×10^{-10}	2.4	1.0
0.1	0.015	10^{-8}	4.4	0.5
0.1	0.015	4×10^{-10}	4.4	0.55
0.05	0.0075	4×10^{-10}	6.7	0.35

Table 3 Maximum reconnection rate E_{max} and time t_0 for complete coalescence for different simulation runs including the ion motion.

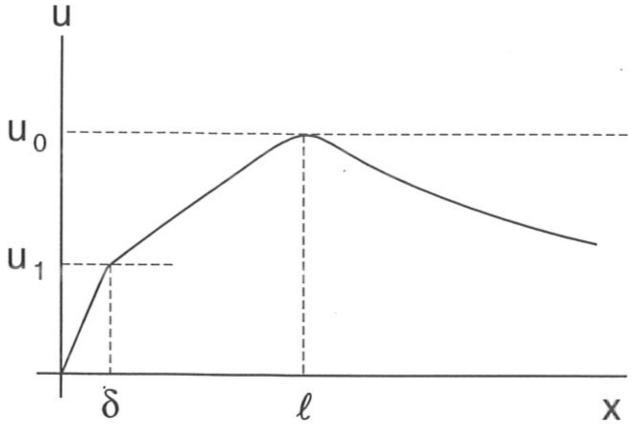

Fig. 1 Upstream velocity profile $v_{ex}(x)$ (schematic drawing).

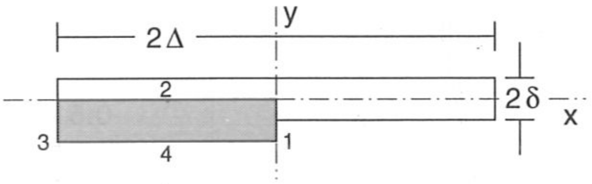
y
2Δ
2δ
x
1
2
3
4

Fig. 2 Integration domain in eq. (26).

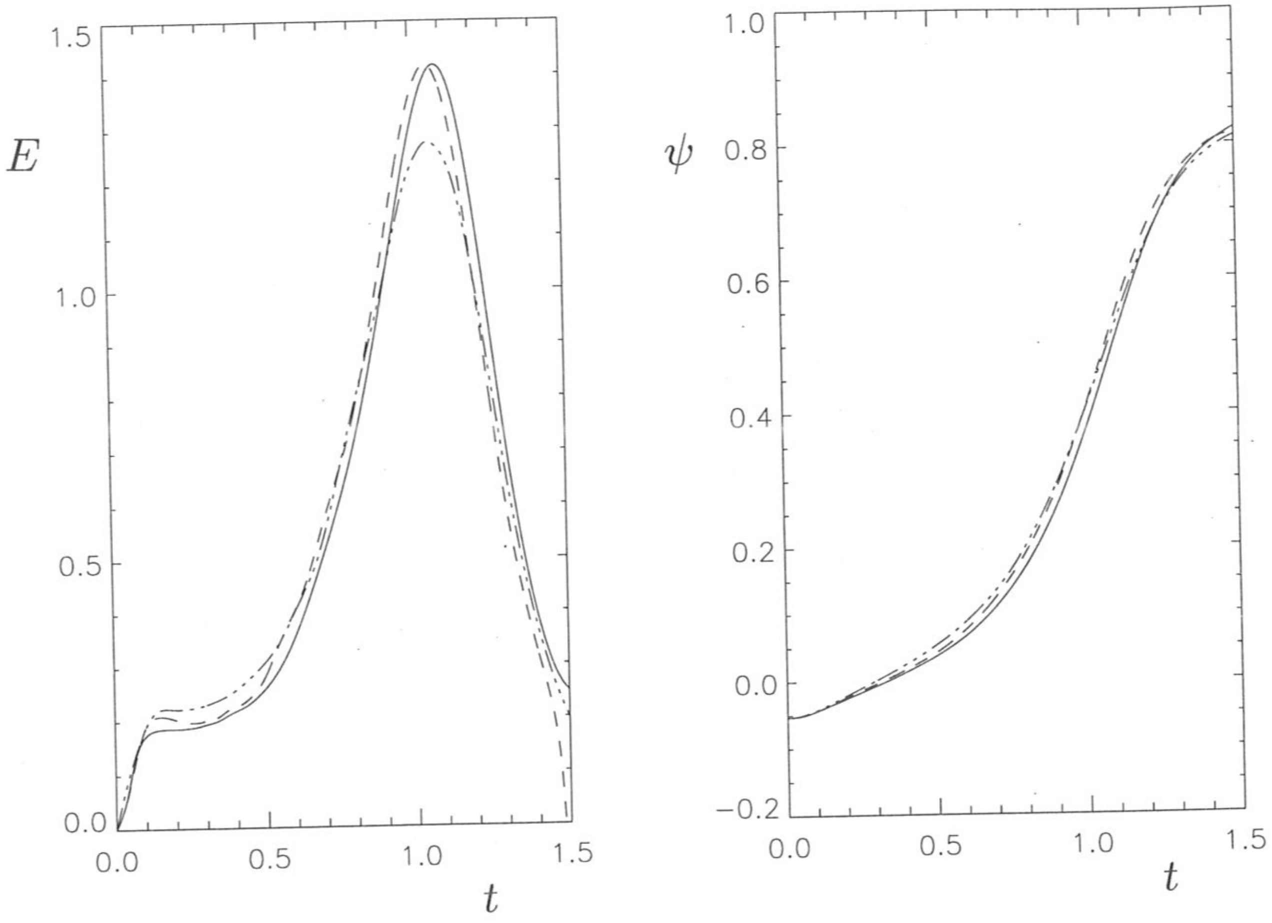

Fig. 3 Time evolution of $E = \partial_t \psi$ and ψ for $d_e = 0.03,\ \eta_3 = 10^{-8}$ —— ; $d_e = 0.03,\ \eta_3 = 5 \times 10^{-10}$ – – – ; $d_e = 0.06,\ \eta_3 = 10^{-8}$ —·-·-— .

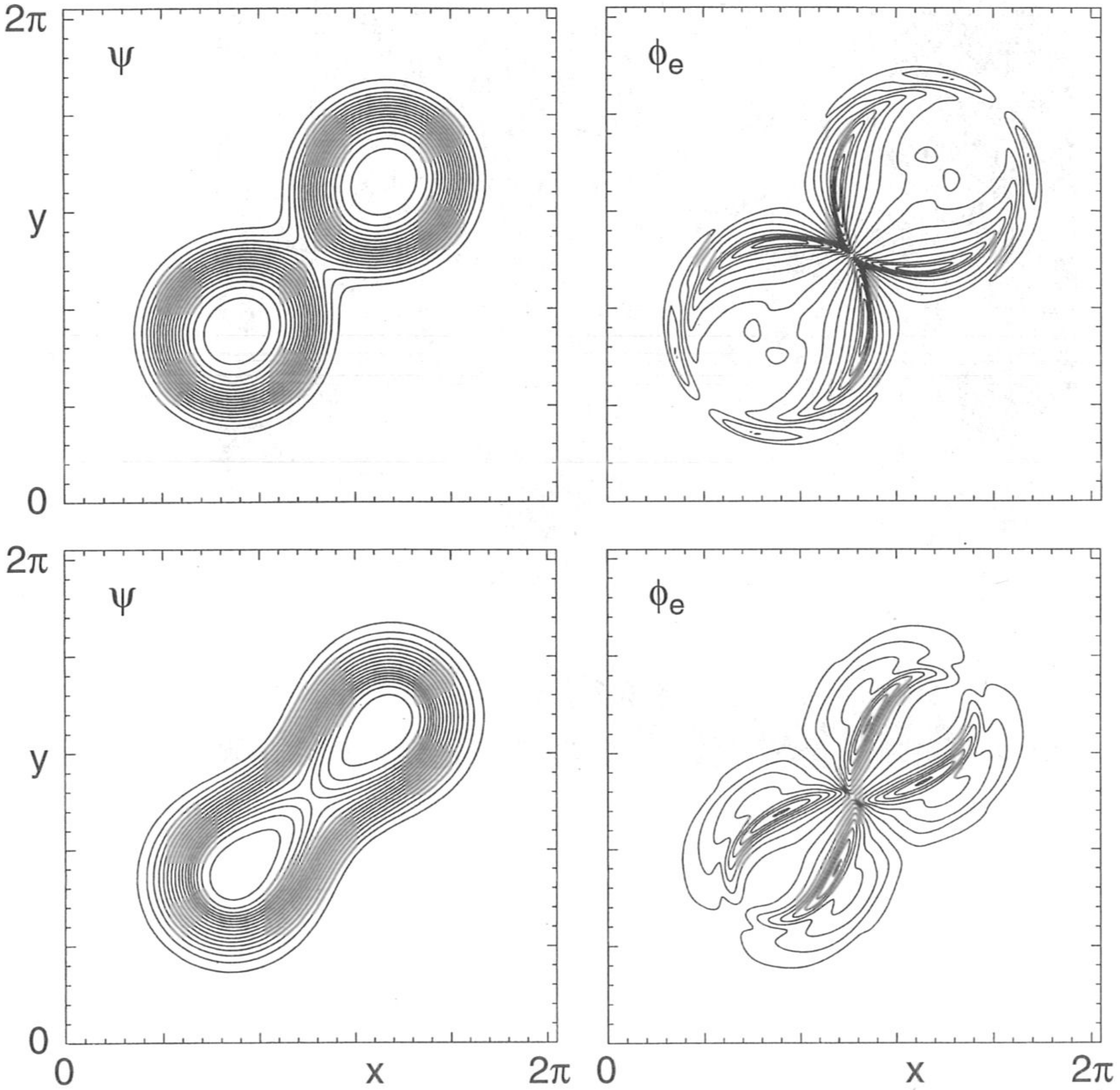

Fig. 4 Coalescence of two flux bundles in EMHD, $d_e = 0.03$, $\eta_3 = 10^{-8}$. Contours of ψ and φ_e for two different times.

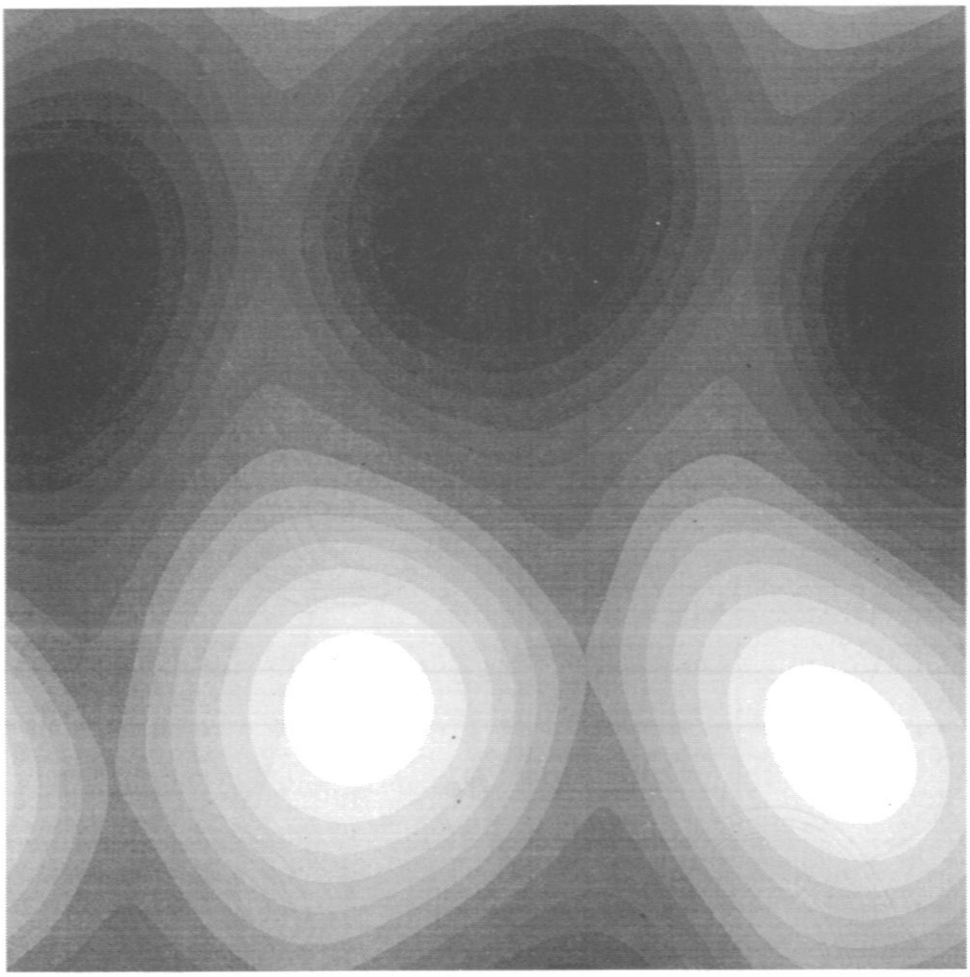

Fig. 5 Generation of whistler turbulence in EMHD reconnection, $d_e = 0.03$. Global view of (a) $\psi(x,y)$, (b) $j(x,y)$; blowups of the region around the lower right X-point (c) ψ, (d) j, (e) ω_e.

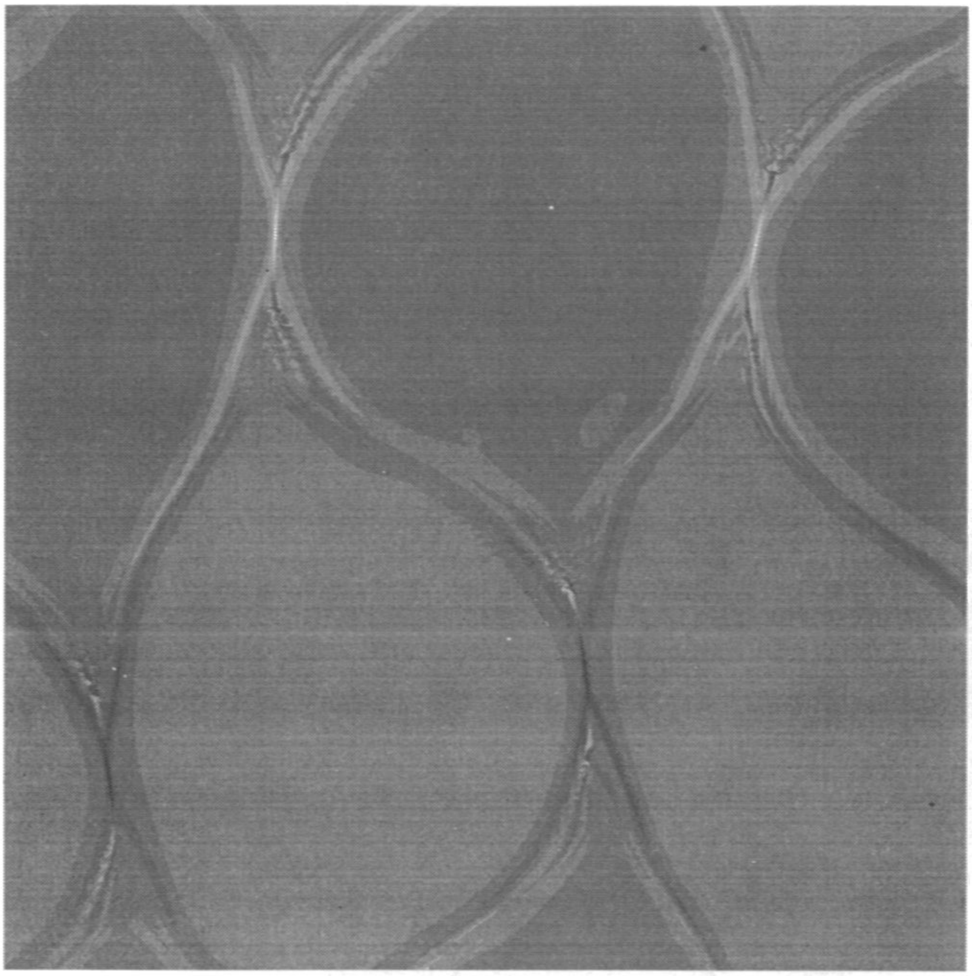

(b)

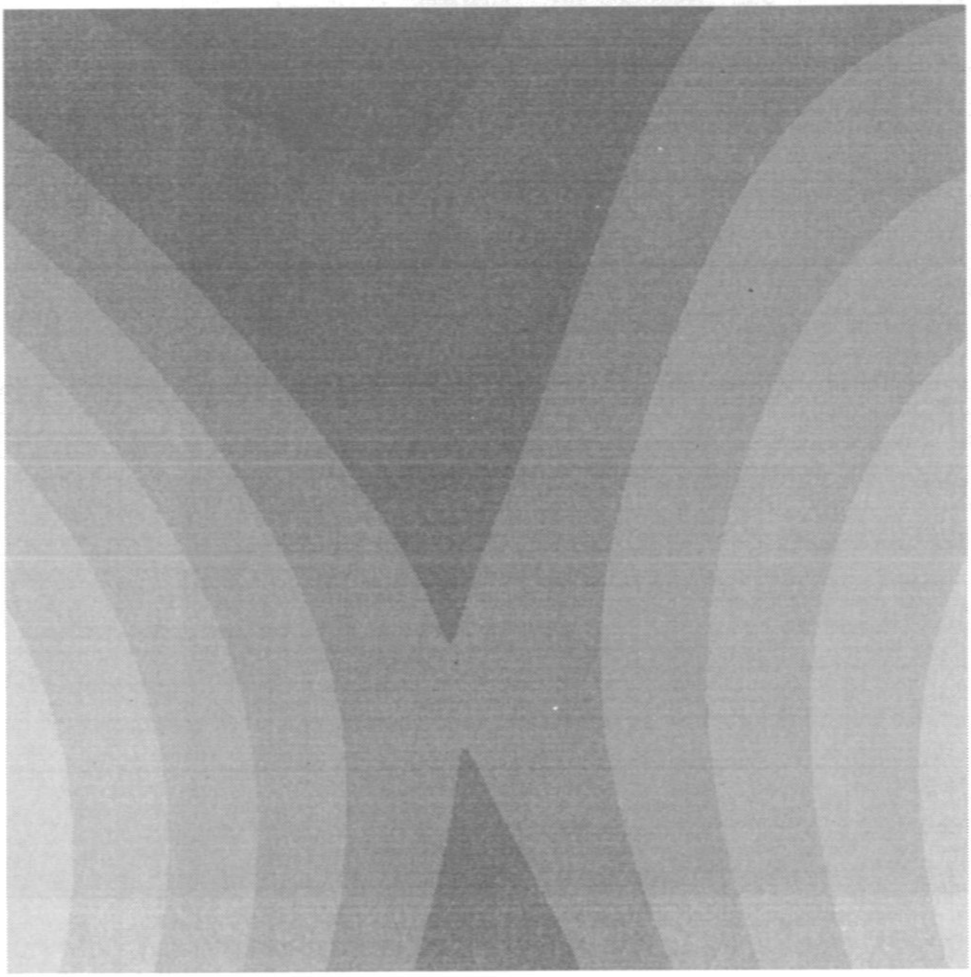

(c)

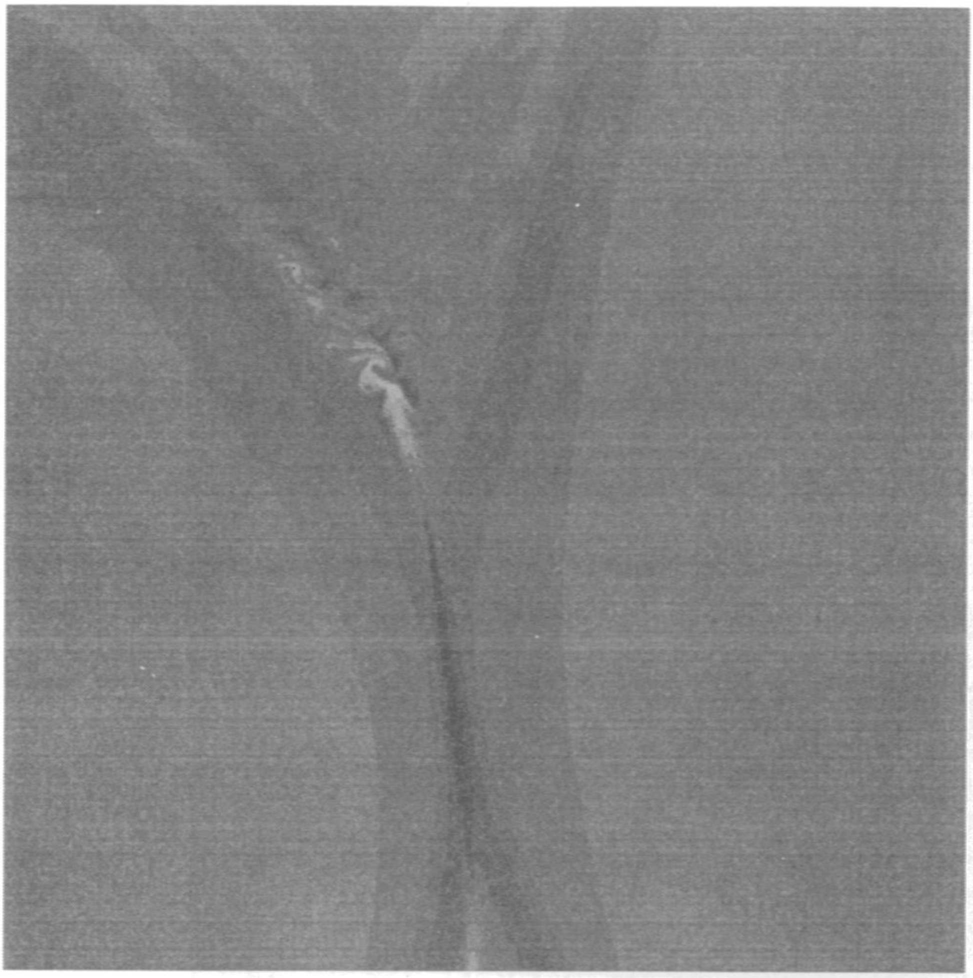

(d)

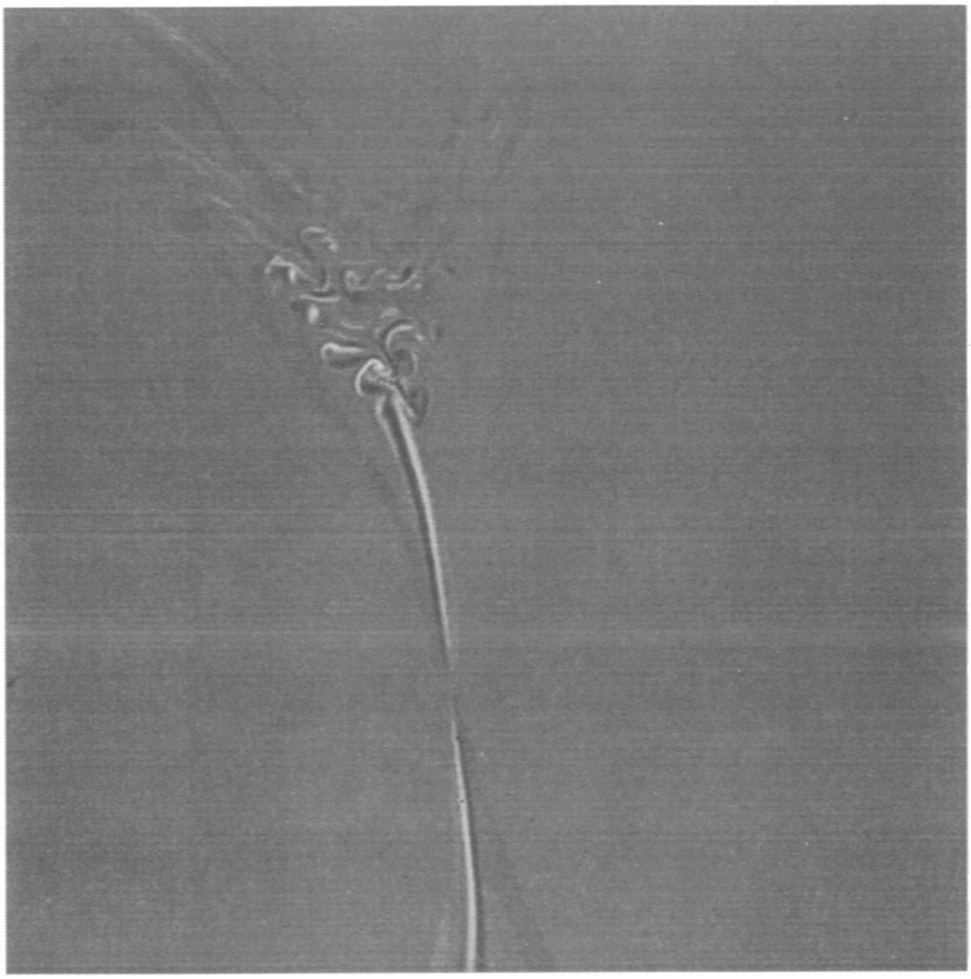

(e)

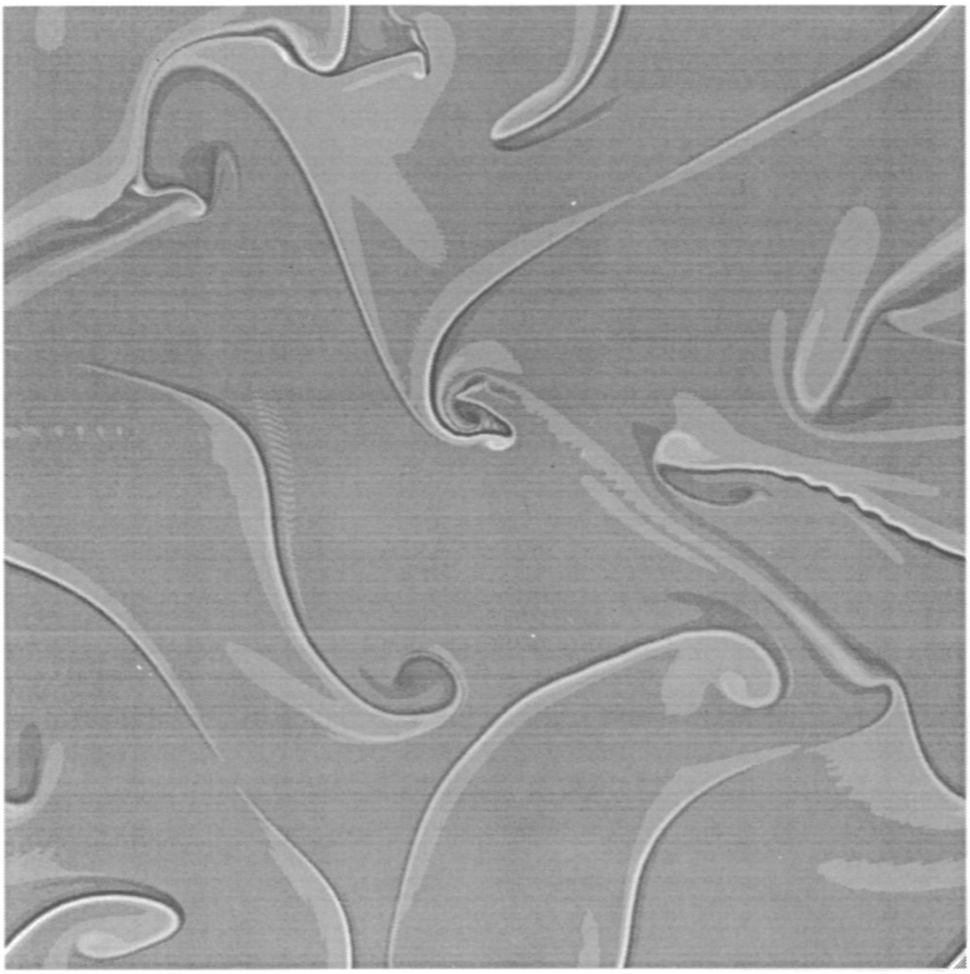

Fig. 6 Generation of whistler turbulence, same initial configuration as in Fig. 4, but $d_e = 1$: $\omega_e(x, y)$ at $t = 2.1$ (a); $t = 3.0$ (b); $t = 4.0$ (c).

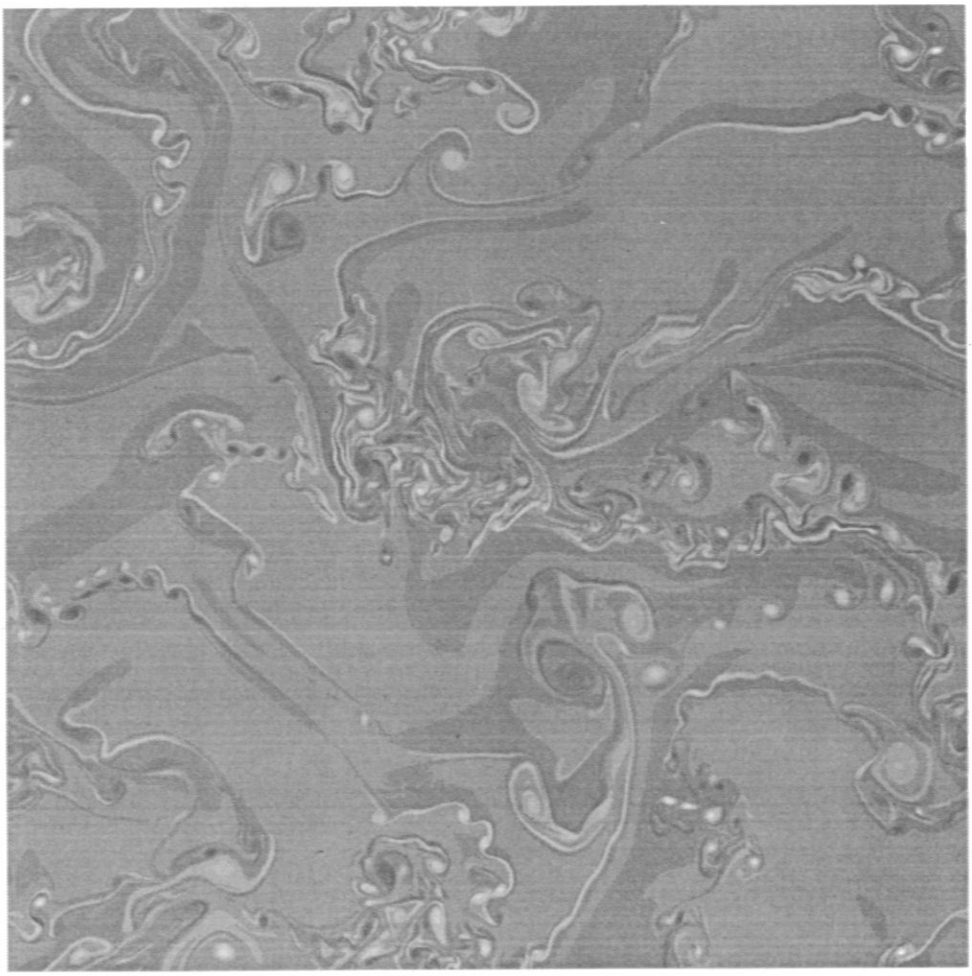

(b)

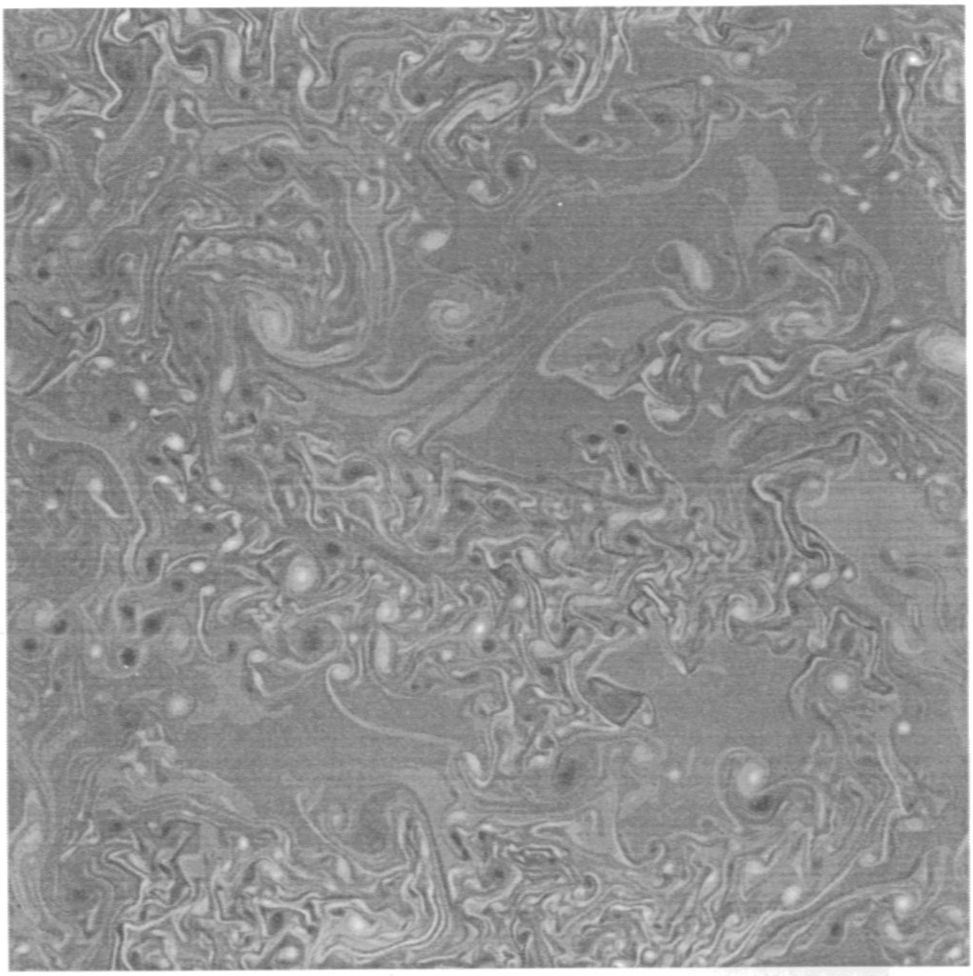

(c)

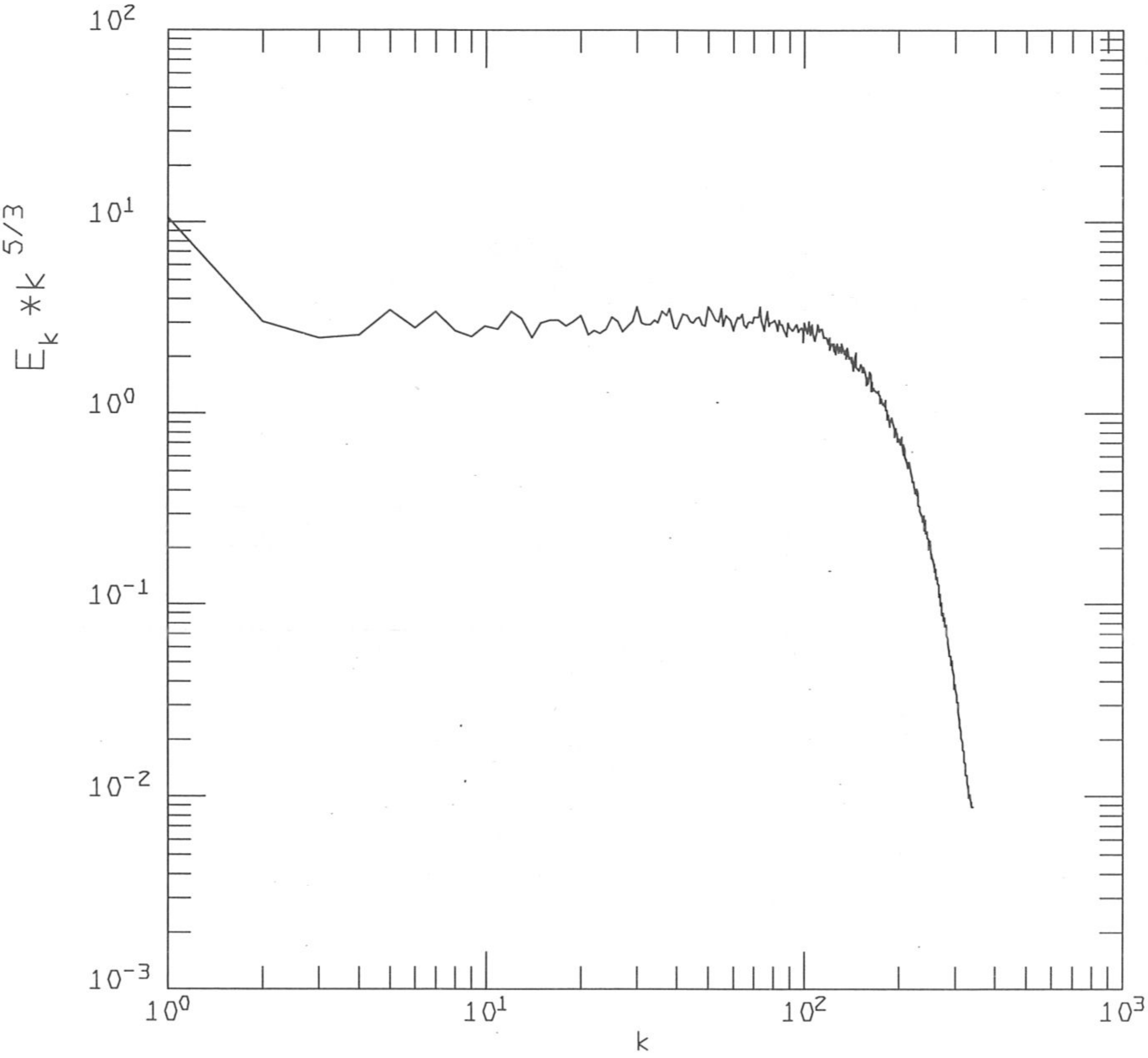

Fig. 7 Compensated energy spectrum $k^{5/3}E_k$ corresponding to the state Fig. 6c.

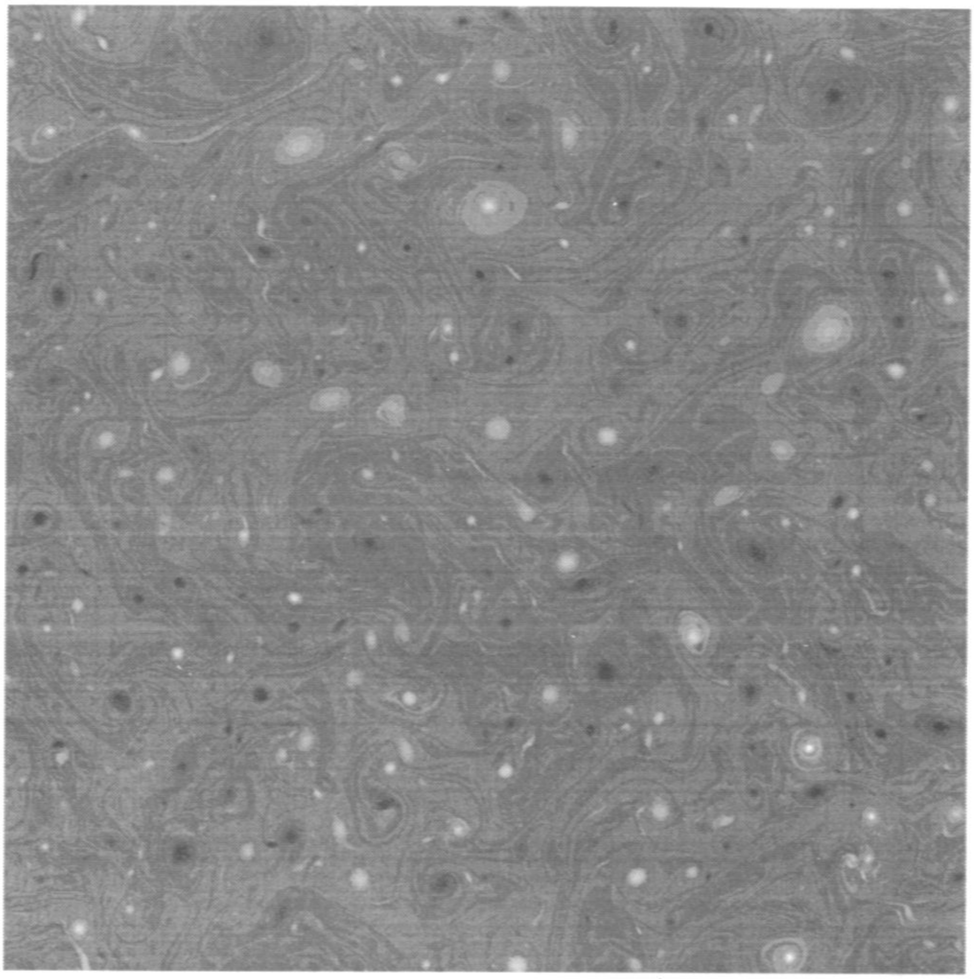

Fig. 8 $\omega_e(x,y)$ at $t=6$, for turbulence decaying from state Fig. 5c with the Lorentz force $\mathbf{B}\cdot\nabla j$ switched off.

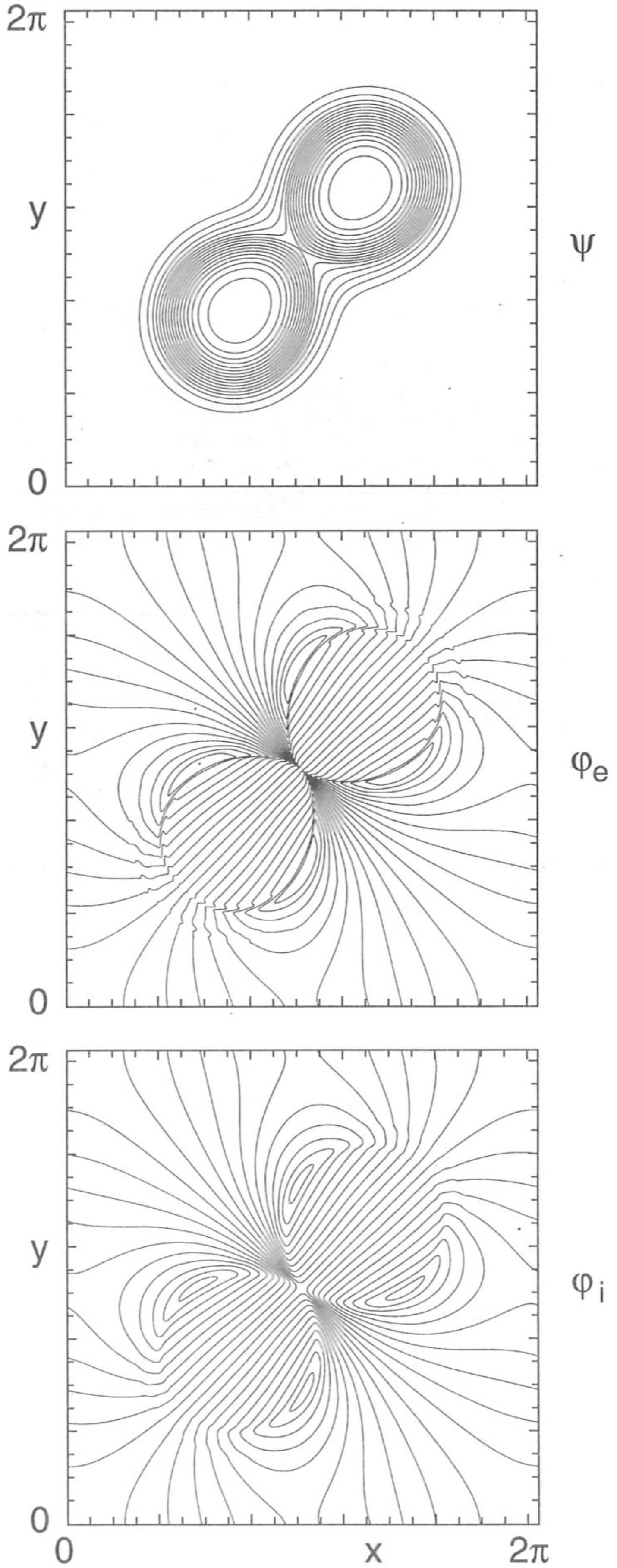

Fig. 9 Coalescence of two flux bundles as in Fig. 3, but including the ion dynamics, $d_i = 0.1$, $d_e = 0.015$, $\eta_3 = 4 \times 10^{-10}$. (a) ψ, (b) φ_e, (c) φ_i.

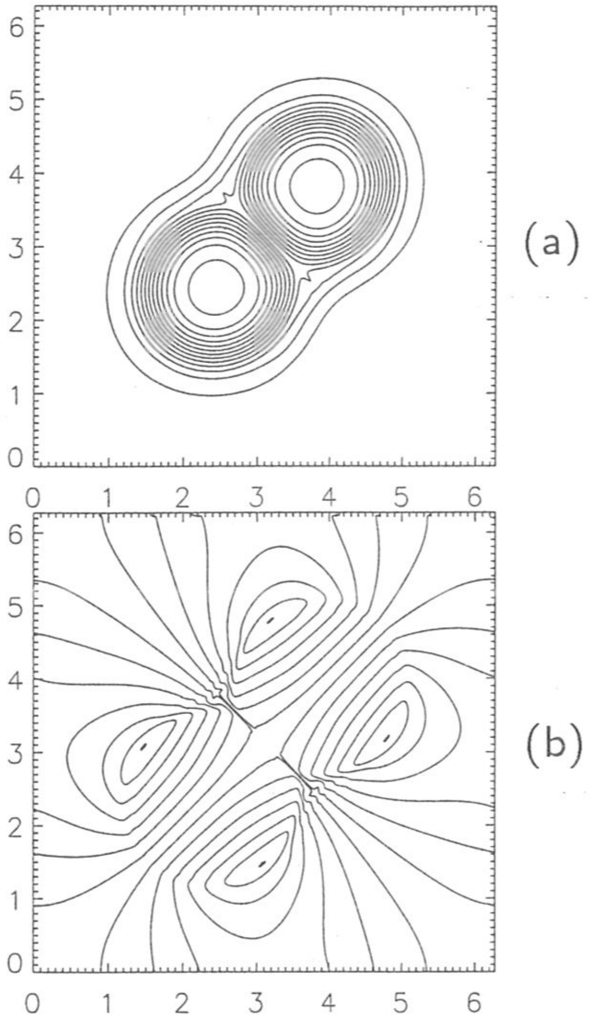

Fig. 10 Coalescence of two flux bundles neglecting the Hall term, $d_e = 0.015$, $\eta_3 = 4 \times 10^{-10}$. Contours of (a) ψ; (b) $\varphi (= \varphi_i = \varphi_e)$.